Earth and Planetary Science Letters 424 (2015) 26–37

Contents lists available at ScienceDirect

Earth and Planetary Science Letters

www.elsevier.com/locate/epsl

Origin of dipping structures in fast-spreading oceanic lower crust offshore Alaska imaged by multichannel seismic data

Anne Bécel [a,*], Donna J. Shillington [a,1], Mladen R. Nedimović [b,a,2], Spahr C. Webb [a,3], Harold Kuehn [b,4]

[a] Lamont Doherty Earth Observatory, Columbia University, P.O. Box 1000, 61 Route 9W, Palisades, NY 10964, USA
[b] Department of Earth Sciences, Dalhousie University, 1459 Oxford Street, P.O. Box 15000, Halifax, Nova Scotia, Canada

ARTICLE INFO

Article history:
Received 21 January 2015
Received in revised form 5 May 2015
Accepted 6 May 2015
Available online xxxx
Editor: P. Shearer

Keywords:
Pacific Plate crust
lower crustal dipping reflectors
Moho discontinuity
oceanic accretionary processes
shear zones

ABSTRACT

Multi-channel seismic (MCS) reflection profiles across the Pacific Plate south of the Alaska Peninsula reveal the internal structure of mature oceanic crust (48–56 Ma) formed at fast to intermediate spreading rates during and after a major plate re-organization. Oceanic crust formed at fast spreading rates (half spreading rate ~74 mm/yr) has smoother basement topography, thinner sediment cover with less faulting, and an igneous section that is at least 1 km thicker than crust formed at intermediate spreading rates (half spreading rate ~28–34 mm/yr). MCS data across fast-spreading oceanic crust formed during plate re-organization contain abundant bright reflections, mostly confined to the lower crust above a highly reflective Moho transition zone, which has a reflection coefficient (RC) of ~0.1. The lower crustal events dip predominantly toward the paleo-ridge axis at ~10–30°. Reflections are also imaged in the uppermost mantle, which primarily dip away from the ridge at ~10–25°, the opposite direction to those observed in the lower crust. Dipping events in both the lower crust and upper mantle are absent on profiles acquired across the oceanic crust formed at intermediate spreading rates emplaced after plate re-organization, where a Moho reflection is weak or absent. Our preferred interpretation is that the imaged lower crustal dipping reflections within the fast spread crust arise from shear zones that form near the spreading center in the region characterized by interstitial melt. The abundance and reflection amplitude strength of these events (RC ~ 0.15) can be explained by a combination of solidified melt that was segregated within the shear structures, mylonitization of the shear zones, and crystal alignment, all of which can result in anisotropy and constructive signal interference. Formation of shear zones with this geometry requires differential motion between the crust and upper mantle, where the upper mantle moves away from the ridge faster than the crust. Active asthenospheric upwelling is one possible explanation for these conditions. The other possible interpretation is that lower crustal reflections are caused by magmatic (mafic/ultramafic) layering associated with accretion from a central mid-crustal magma chamber. Considering that the lower crustal dipping events have only been imaged in regions that have experienced plate re-organizations associated with ridge jumps or rift propagation, we speculate that locally enhanced mantle flow associated with these settings may lead to differential motion between the crust and the uppermost mantle, and therefore to shearing in the ductile lower crust or, alternatively, that plate reorganization could produce magmatic pulses which may lead to mafic/ultramafic banding.

Published by Elsevier B.V.

1. Introduction

Oceanic lithosphere produced at mid-ocean ridges covers 70% of Earth, yet fundamental questions remain about mantle flow and melt migration at mid-ocean ridges, and the mechanism(s) of crustal accretion. Is the crust accreted from a single mid-crustal axial magma lens with passive mantle flow (e.g., "gabbro glacier" model, Phipps Morgan and Chen, 1993; Quick and Denlinger, 1993) or in situ through the injection of a series of sills through-

* Corresponding author. Tel.: +1 845 365 8648.
E-mail addresses: annebcl@ldeo.columbia.edu (A. Bécel), djs@ldeo.columbia.edu (D.J. Shillington), mladen@dal.ca (M.R. Nedimović), scw@ldeo.columbia.edu (S.C. Webb), Harold.Kuehn@dal.ca (H. Kuehn).
[1] Tel.: +1 845 365 8818.
[2] Tel.: +1 902 494 4524.
[3] Tel.: +1 845 365 8439.
[4] Tel.: +1 902 494 3673.

http://dx.doi.org/10.1016/j.epsl.2015.05.016
0012-821X/Published by Elsevier B.V.

out the crust (e.g., "sheeted sill" model, Boudier et al., 1996; Kelemen et al., 1997)? How active is the mantle upwelling beneath mid-ocean ridges (e.g., Forsyth, 1992; Blackman and Kendall, 2002)? Magmatic and mantle flow processes exert control on the deformation style of the crust and upper mantle at and near the ridge axis and thus on the seismic structure of the crust.

Fast-spreading mid-ocean ridges have axial highs and a thin axial magma lens (AML) characterized by significant melt content that is underlain by the axial magma chamber (AMC). The AMC is a 5- to 10-km-wide partially molten zone with significant interstitial melt that extends to the base of the crust (Vera et al., 1990; Kent et al., 1993; Dunn et al., 2000; Zha et al., 2014). Off axis magma lenses have also been recently imaged as bright mid-crustal reflections beneath the flanks of the East Pacific Rise (EPR) and at the Moho transition zone here (Canales et al., 2012; Han et al., 2014) in apparent contradiction to the predictions of the gabbro glacier model. However, the contribution of off-axis magma bodies to the formation of lower oceanic crust remains unclear. After its formation, the oceanic lithosphere cools and sinks away from the ridge axis. Convective hydrothermal circulation at the ridge axis and on ridge flanks facilitates cooling of upper oceanic crust until it is shut off by sediment blanketing. Debate continues about the roles of conductive cooling and penetration of seawater derived fluids in lower crustal cooling (e.g., McCulloch et al., 1981; Bosch et al., 2004). Cooling of the oceanic lithosphere can eventually generate thermal stresses that lead to cracking and fissuring (e.g., Parmentier and Haxby, 1986), which can further modify the off-axis fluid flow and contribute to continued cooling (e.g., Fisher, 1998; von Herzen, 2004).

Little is known about the structure of and aging processes in old oceanic crust due to the lack of data; most studies have focused on the ridge axis, fracture zones and seamounts, or at convergent and rifted margins. Most of the few MCS profiles across old, mature oceanic crust reveal dipping reflections in the lower crust (e.g., Ranero et al., 1997), but their origin still remains enigmatic. In most data from old oceanic crust formed at the slow-spreading Mid-Atlantic Ridge, some crustal reflections appear to continue through the entire crust and directly correlate to rough topography, so they are mainly attributed to large-scale extensional faulting (Mutter et al., 1985; NAT Study Group, 1985; McCarthy et al., 1988; White et al., 1990; Mutter and Karson, 1992; Morris et al., 1993; McBride et al., 1994).

Lower crustal reflections are also observed in data collected across fast spread crust in the Pacific Ocean (Eittreim et al., 1994; Ranero et al., 1997; Reston et al., 1999) that differ from those observed in slow-spreading crust in that they are confined to the lower crust and are not clearly related to offsets at the top or base of the crust. Consequently, they were attributed to either compositional layering (mafic/ultramafic banding) (e.g., Ranero et al., 1997) that has been observed in ophiolites and modeled to form by ductile flow from the AML with a passive mantle upwelling (e.g., Henstock et al., 1993; Phipps Morgan and Chen, 1993) or secondary shear zones generated in the ductile lower crust in response to a basal shear applied at the Moho transition zone (MTZ) by active mantle upwelling (Nicolas et al., 1994; Kodaira et al., 2014). Some studies invoke both near-axis processes/deformation and off-axis crustal aging (Hallenborg et al., 2003).

The described studies provide fundamental constraints on the structure of fast-spreading oceanic crust and the processes involved in its formation and evolution, but they leave several core questions unanswered. Many authors interpret dipping reflections as shear zones (Ranero et al., 1997; Kodaira et al., 2014), which appear to require some form of active upwelling. However, modeling and other observations at fast-spreading ridges suggest that upwelling is passive in these settings (Parmentier and Phipps Morgan, 1990; Blackman and Forsyth, 1992; Forsyth, 1992) although the pattern of mantle upwelling is still debated (Carbotte et al., 2004).

In this paper, we present MCS reflection images from the ALEUT (Alaska Langseth Experiment to Understand the megaThrust) experiment of the North Pacific oceanic crust offshore Alaska Peninsula, which surveys crust formed at both fast and intermediate spreading rates. We focus on the origin of lower crustal reflections by combining constraints from MCS data on the geometry, internal structure, amplitude and distribution of these events. We estimate the absolute reflection coefficients for the brightest events, which we use to test explanations for their amplitude. Our results, combined with published work, illuminate possible controls on the dipping events imaged in the lower oceanic crust such as spreading rate, mantle flow, plate reorganizations, and aging.

2. Geological setting and seafloor spreading history

The Pacific oceanic crust examined in this study formed in the late Tertiary (48 to 56 Ma) at fast to intermediate spreading rates and is currently located near the present day boundary between the North American and the Pacific plates (Fig. 1). This oceanic crust records significant variations in the direction and rate of spreading due to major plate reorganizations (Lonsdale, 1988). At ∼56 Ma (chron 25), a major plate reorganization occurred involving a reorientation of the Kula ridge and a jump in the Kula–Pacific–Farallon triple junction (Lonsdale, 1988; Seton et al., 2012). Plate reorganization was accompanied by an increase of the spreading rate (74 mm/yr half rate, Engebretson et al., 1984; 54 mm/yr half rate, Lonsdale, 1988) at the Pacific–Kula ridge and is preserved in unsubducted oceanic crust off the Alaska Peninsula. The fossil triple junction left behind by the reorganization is located at the T-shaped Anomaly 24.2 (53 Ma) (Fig. 1). Anomalies to the east of 158°W, younger than chron 23 (52 Myr) appear to reflect the intermediate Pacific–Farallon spreading rate (∼28–34 mm/yr, half rate) accreted after plate reorganization (Engebretson et al., 1984).

Of the ALEUT data seaward of the trench, Lines 5, 6 and 23C are near perpendicular to the magnetic anomalies and thus approximately coincide with the flow lines and provide a record of the processes of crustal accretion at fast and intermediate spreading rates (Fig. 1). Line 4 crosses the fossil triple junction (Nedimović et al., 2011; Bécel et al., 2012), Line 2 crosses the Patton–Murray seamount chain, and Line 6 passes near the center of a small seamount. The profiles shown here were chosen to avoid areas affected by subduction (∼60 km from the trench) and triple junction processes. However, as described later, the triple junction might have played a role in the formation of the lower crustal dipping events at the time of the crustal accretion.

3. Data acquisition

Data used in this study were collected by the R/V *Marcus G. Langseth* in summer 2011 for the ALEUT program. The survey imaged the subduction zone system, including the incoming oceanic plate ∼60–130 km seaward of the trench, before it was modified by bending and subduction (Fig. 1). In total, we acquired 3700 km of MCS data with two 636-channel, 8-km-long streamers and a 6600 cu. in. tuned 36-element airgun array (Fig. 1). The source and one of the streamers were towed at 12 m to maximize low frequencies and deep imaging while the second streamer was towed at 9 m for better imaging of the sediments and upper crust. The shot interval for the MCS data acquisition was 62.5 m and the group spacing 12.5 m resulting in nominal common midpoint (CMP) bin spacing of 6.25 m, and CMP data trace fold of 64. The long record length (22 s) allows us to fully capture the seafloor multiple needed for calibration and estimation of true reflection

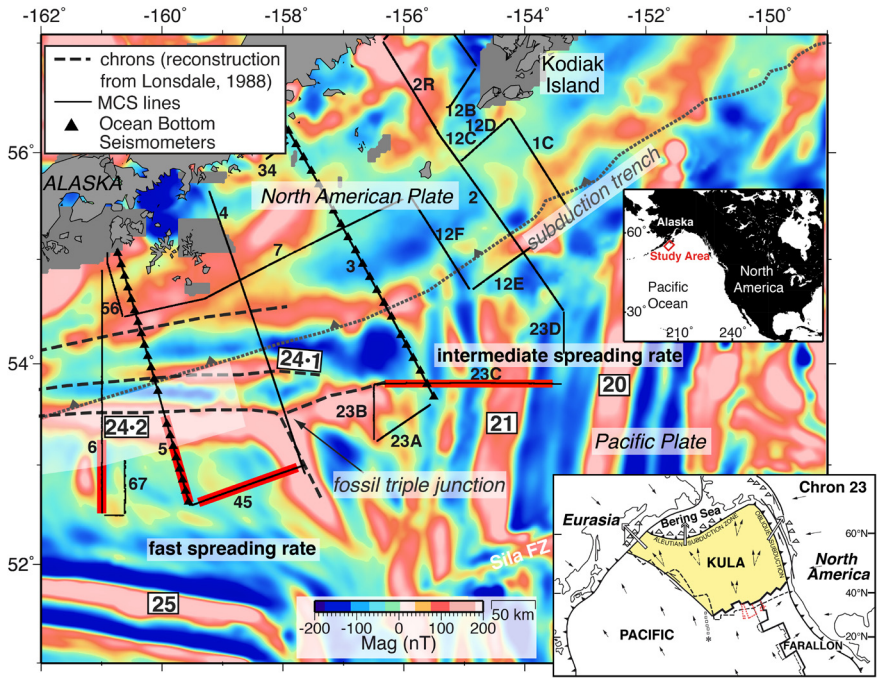

Fig. 1. ALEUT experiment location shown with magnetic anomalies. Dark grey dashed lines and numbers in white boxes indicate the preferred reconstruction with the chron numbers from Lonsdale (1988). Light grey dotted line is the subduction trench. Thin black lines and numbers show the MCS profiles, and the black triangles represent the ocean bottom seismometers. The MCS profiles analyzed for this study are highlighted by thick red lines. The part of the oceanic crust affected by subduction processes such as bending related faulting and/or flexural bulge is shaded in white for profiles 5 and 6. The inset in the top-right corner of the map shows the location of the study area with respect to the Pacific Ocean. The inset in the bottom right corner illustrates the plate configuration at chron 23 after plate reorganization (after Lonsdale, 1988). (For interpretation of the references to color in this figure legend, the reader is referred to the web version of this article.)

coefficients. Sampling rate was 2 ms, resampled to 4 ms for processing after applying an anti-aliasing filter. The analyzed signal has a bandwidth of ~3 to 125 Hz.

Two ~300-km-long ocean bottom seismometer (OBS) refraction lines were shot coincident with MCS profiles 3 and 5 using 21 Scripps Institution of Oceanography (www.obsip.org) short-period 4-component instruments spaced at ~15–18 km. The OBS lines extend up to 100 km away from the trench allowing for good sampling of the oceanic velocity-depth structure prior to bending and subduction (Shillington et al., 2013).

4. MCS data processing

All MCS profiles shown here (Figs. 2–5) were generated from data acquired with the 12-m-deep streamer and processed with Paradigm software (Focus and Geodepth). MCS processing included CMP bin geometry, band-pass filtering (3–7–100–125 Hz), spherical divergence correction, noise suppression using the LIFT method (Choo et al., 2004), predictive deconvolution to remove low frequency ringing of the source signal due to the residual bubble pulse, velocity analysis, parabolic radon transform for removal of the basement signal scattering and internal multiples within the crust, pre-stack time migration using a smoothed version of the RMS velocities, outer mute, residual moveout correction and migration summation, with time variant filtering, seafloor mute and time variant gain for display purposes. Line 23C (Fig. 3) is post-stack time migrated.

5. Results

5.1. Sediments, basement topography and upper crust

The thickness of the sediment varies from ~35 to ~850 m among and along profiles across fast-spreading crust assuming an average velocity of 1.8 km/s (Figs. 2, 3 and 4). The basement topography is very smooth, with variations up to 150 m over 3–10 km. Relative changes in roughness are observed along Line 6 (CMP 39 800, Fig. 4) and Line 45 (CMP 32 100, Fig. 2a). Basement topography is substantially rougher for oceanic crust created at intermediate spreading rate, with variations of up to ~800 m over distances of 1–14 km (Fig. 5a), similar to intermediate spreading crust elsewhere (e.g., Malinverno, 1991). For oceanic crust created at intermediate spreading rate, sediment thickness changes from 10's of m to 1.5 km over short distances (Fig. 5).

Near vertical faults are identified in the sediments over both fast and intermediate spreading crust (e.g., Figs. 2a, 5a), but are more abundant over the latter. These faults are characterized by very small throws that may be caused by differential sediment compaction associated with igneous basement topography, by reactivation of normal crustal faults formed at the spreading center, or by both processes (Nedimović et al., 2009).

We observe locally bright, short reflection segments in the upper 1–1.2 s beneath the basement in fast-spreading crust that are irregularly spaced and dip in both directions (Figs. 3b, 4b, 5b). Some reflections appear to be linked to small disruptions at the top of the oceanic crust. There is no clear continuity between the upper and lower crustal reflections except at a couple of locations (e.g., Figs. 2b, 2e, CMPs 25 500–26 300). The mid crust is acoustically almost transparent.

5.2. Dipping reflections in the lower oceanic crust

All ALEUT MCS data across fast spreading oceanic crust formed during plate reorganization contain abundant bright dipping reflections confined to the lower crust (e.g., Fig. 2b). Nearly all of these dipping events vanish in the middle crust (1–1.2 s twtt below basement) and either terminate at the Moho discontinuity or sole out into it with shallowing dips. These reflections appear to dip in the direction of the paleo-ridge axis; events on Line 6 have

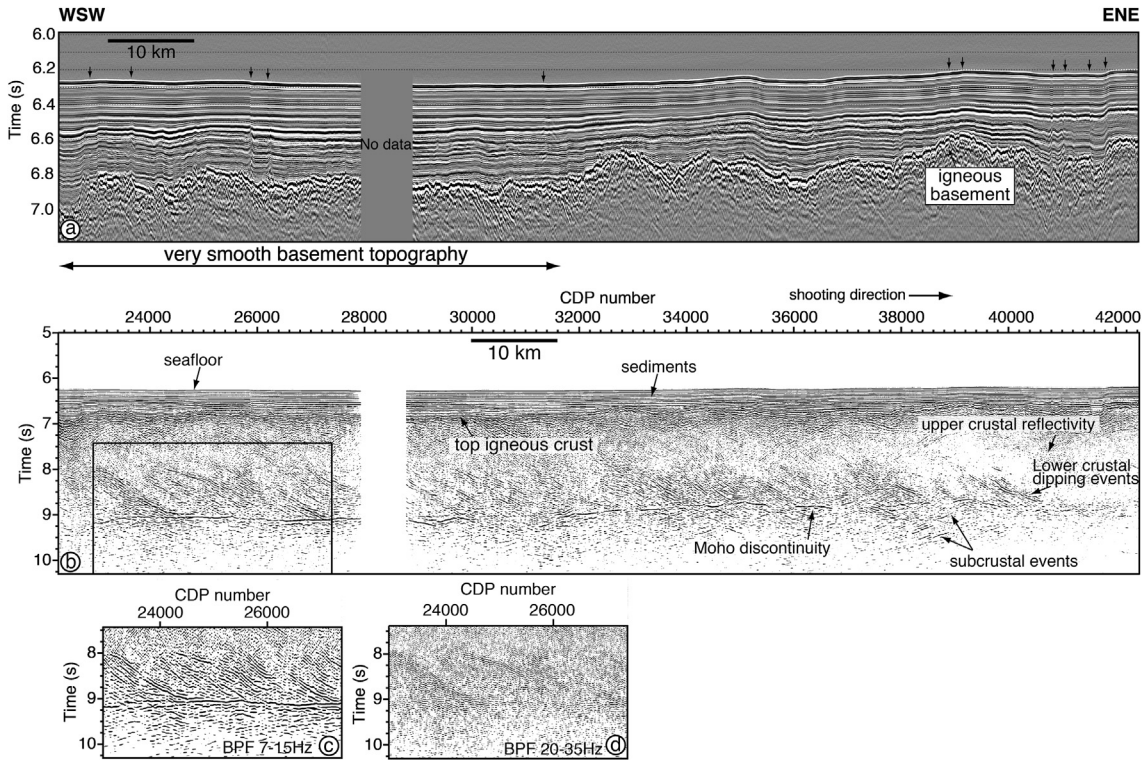

Fig. 2. Reflection images of Line 45 across fast spread crust. (a) Post stack time migrated section showing moderate faulting within the sediments indicated by small black arrows. (b) Pre-stack time migrated section showing dipping events in the lower crust above a bright MTZ. Black rectangular box marks the section of the pre-stack migrated section that has been filtered in panels c and d. (c) Panel of the prestack migrated stack section filtered between 7 and 15 Hz. (d) Panel of the stack section filtered between 20 and 35 Hz.

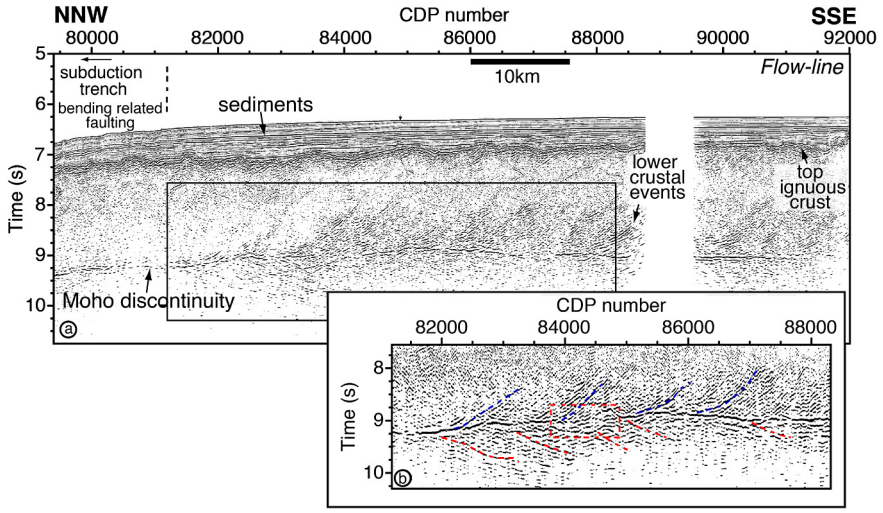

Fig. 3. Reflection images of Line 5 across fast spread crust. This profile approximately coincides with the flow lines. (a) Pre-stack time migrated section. Black rectangular box marks part of the section filtered in panel b. (b) Part of the prestack time migrated section band-pass filtered between 7 and 15 Hz. Lower crustal dipping events are indicated in blue and dipping events in the uppermost mantle in red. (For interpretation of the references to color in this figure legend, the reader is referred to the web version of this article.)

slightly higher dips than Lines 45 and 5, possibly because Line 6 is closer to being orthogonal to the N–S paleo-spreading direction (Fig. 1). However, it is possible that some of the events may dip E–NE towards the fossil triple junction. Depth converted MCS profiles give apparent dip angles for lower crustal events of ~10 to 30°. The most prominent dipping events can reach lengths of 1.5–2 s twtt or ~5 to 7 km assuming a velocity of 7 km/s. Many short (1- to 5-km-long) dipping events are observed that exhibit both relatively low (7–15 Hz) and high (20–35 Hz) frequencies, indicating that the signal frequency band is broad (Figs. 2c and 2d).

There is no clear evidence of a systematic reverse or normal polarity of the lower crustal dipping reflectors with respect to the seafloor reflection in the stack or pre-stack domains. These reflections may represent “discrete” events but no obvious regularity in spacing is observed as suggested by previous studies and attributed to, for example, periodicity in magmatic processes (Eittreim et al., 1994; Reston et al., 1999). Dipping events are best imaged where the overlying basement is smooth. There is no clear relationship between offsets in the basement and the dipping events except at a few locations where dipping reflections are im-

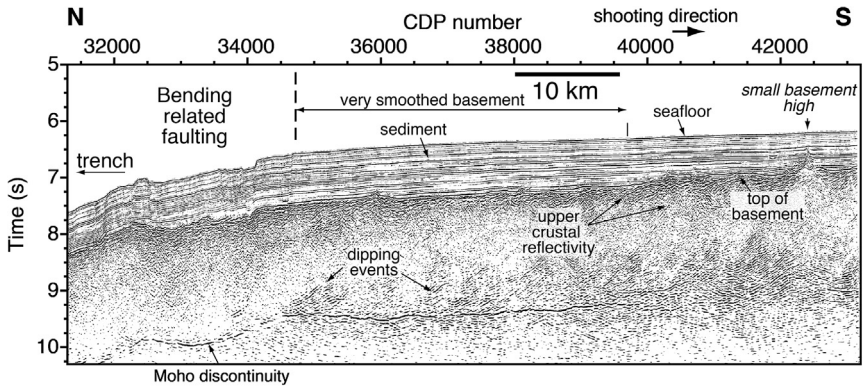

Fig. 4. Pre-stack time migrated section of Line 6 across fast spread crust. This profile is an approximate flow line. Note the very smooth basement and the bright and continuous MTZ at which the dipping events terminate, CMP 34 700–39 600.

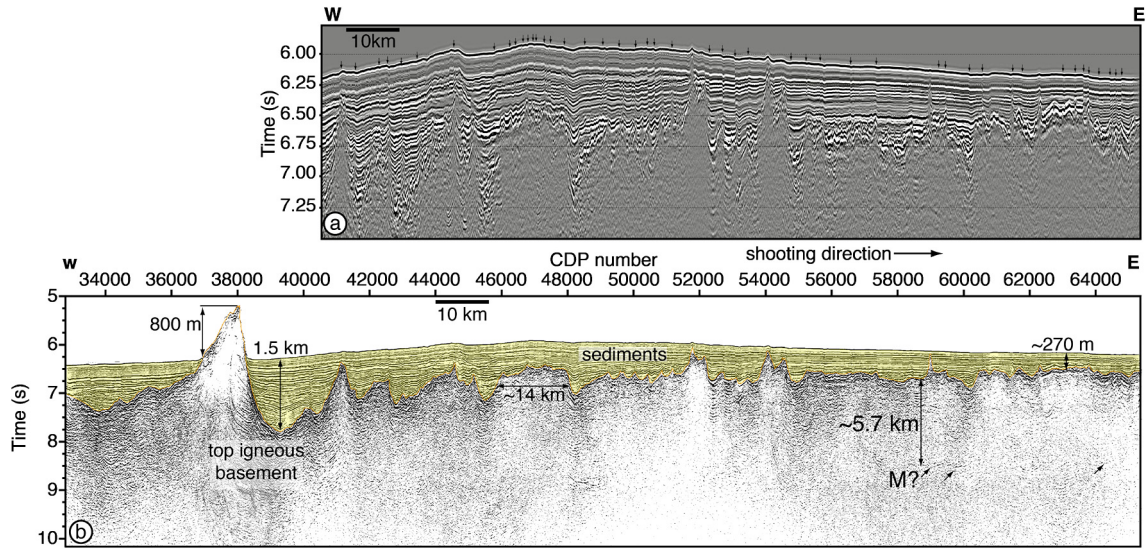

Fig. 5. (a) Section of the post-stack time migrated Line 23C across intermediate spread crust showing abundant faulting within the sediments above a reflective, high topography basement. (b) Post-stack time migrated Line 23C. Yellow shading represents the sediment cover. This profile is an approximate flow line. (For interpretation of the references to color in this figure legend, the reader is referred to the web version of this article.)

aged as continuous events across offsets in the basement. In some areas, irregular patterns and cross-cutting relations between events are observed (e.g., Fig. 2b, CMP 34 000–35 000) especially when the basement is rougher and reflections from the Moho transition zone are weaker or absent (e.g., Fig. 4 CMP 40 500–42 000). In areas with basement offsets caused by faulting, this may be due to the increased crossdip component of the imaged structures, which is not accounted for by standard 2D analysis of feathered data (Nedimović and West, 2003a).

Most of the dipping events terminate at the MTZ. In a few places, dipping reflectors appear to cross the Moho reflection without offsetting it (e.g., Fig. 2b, CMP 34 000–36 300). The absence of a clear step in the Moho may reflect incomplete migration of the dipping events oriented obliquely to the profile (Nedimović and West, 2003b).

On Lines 5 and 6 (Figs. 3, 4), lower crustal dipping events vanish to the north. For Line 5, dipping events stop at magnetic anomaly 24.2 (∼CMP 81 500), which also coincides with the onset of bending faulting. On Line 6, dipping events are still observed in the area of bending related faulting but are less clearly imaged, probably because these reflectors become too steep and/or are disrupted by bending faulting.

We do not observe dipping reflections in the lower crust on profiles crossing crust formed at the intermediate spreading rate after plate reorganization (Fig. 5b). It is possible that scattering associated with rougher basement topography could impede imaging of features in the crust. However, the acquisition parameters are the same, and we image the Moho and other crustal structures clearly in other areas of rough topography suggesting we would see such features in intermediate spreading crust if present.

5.3. Moho discontinuity and subcrustal events

The MTZ reflections arrive 2.25 s twtt (±0.2 s) after the basement reflection along all ALEUT profiles crossing fast-spreading crust, which indicates a crustal thickness of 6.9 ± 1.4 km assuming an average velocity for the whole crust of 6.2 km/s (Spudich and Orcutt, 1980); this is consistent with the crustal thickness from the refraction modeling (Shillington et al., 2013). The uniform crustal thickness on all profiles crossing fast spreading crust suggests steady state magma production or at least minimal fluctuations at the time of crustal accretion and minimal crustal thickening by off-axis magmatism.

Over most of the fast spreading crust, the MTZ is a strong and sharp event that is laterally continuous for ∼10 s of km (e.g., Figs. 2b and 2c, CMP 24 000–27 500). However, in some areas the MTZ is more complex in shape and thickness (e.g., Fig. 2b, CMP 28 600–29 000) and/or becomes less reflective (e.g., Fig. 2b, CMP 30 000–310 000 or 41 000–42 000). In a few places, changes in MTZ reflection character could be explained by basement scattering and

defocussing of energy. Examples include changes in character beneath 1) a small basement high (e.g., Fig. 4, CMP 40 000–42 000) and 2) basement topography changes on Line 45 (Fig. 2, CMP 32 000). However, there is considerable variability in the strength and character of the Moho that is not easily attributed to scattering or defocussing and thus must arise from changes in physical properties.

The crust–mantle transition appears much less reflective on the profiles over intermediate spreading crust (Fig. 5b). Here, the inferred average crustal thickness is only ∼5.6 km (∼1.8 s twtt). Crustal thickness appears to vary laterally and basement topography is rougher. The diminished or absent MTZ reflection could be due to basement scattering, attenuation or absorption of the energy by the seafloor, sediment, or overlying crust, or it may also indicate a lack of impedance contrast at this discontinuity and a more gradual increase in velocity with depth as, for example, observed at a location near the fast spreading rate East Pacific Rise (Vera et al., 1990).

Subcrustal events are seen below the MTZ (Figs. 2, 3 and 4) only on profiles across fast spreading crust. They dip gently at ∼10–18° mostly in the opposite direction of the lower crustal events (i.e., away from the paleo-ridge axis). The most prominent events are imaged on Line 45 (Fig. 2, CMP 37 500–40 500), where the Moho is rather discontinuous and the geometry of the lower crustal reflections is more complex.

5.4. Reflection coefficients

The high signal-to-noise ratio of the ALEUT dataset allows us to clearly identify the brightest lower crustal and MTZ reflections in the pre-stack domain and to constrain their absolute reflection coefficients (Fig. 6 and Suppl. Fig. 1). These are the first constraints on the absolute reflection coefficients of the dipping lower crustal events. The amplitudes are first corrected for geometrical spreading. Although every effort has been to made to ensure signal amplitude loss is minimized during noise suppression, the calculated absolute reflection coefficients may be smaller than the true reflection coefficients. As in many other studies, the water bottom multiple was used to calibrate the amplitude of the input signal (White, 1977; Warner, 1990). Reflection coefficients were estimated for the largest and most prominent lower crustal events with the lowest dips and for the Moho reflections on near traces (offsets of <2000 m) in CMP gathers so that the angle of incidence is negligible.

We calculated reflection coefficients of 0.12 for the seafloor and 0.4 for the basement, which is more than 3 times greater than for the seafloor. We estimated a reflection coefficient of 0.092 for one of the brightest dipping events and of 0.08 for the Moho. These estimates were then corrected for intrinsic attenuation assuming a dominant frequency of 20 Hz and Q of 100 (Mithal and Mutter, 1989) for the sediments, Q of 400 and 1500 for the upper and lower crust respectively (Mithal and Mutter, 1989; Minshull and Singh, 1993). Reflection coefficients corrected for attenuation reach 0.58 for the basement, 0.15 for the dipping reflection, and 0.13 for the MTZ. The amplitudes of the brightest dipping events are thus greater than or equal to those of the Moho.

The computed reflection coefficient for the Moho could, for example, indicate a velocity jump from 7.0 km/s to 8.1 km/s, which are characteristic values of lower crustal gabbros and uppermost mantle peridotites (Bée and Bibee, 1989; Fujie et al., 2013; Kodaira et al., 2014, and Shillington et al., 2013) and a density jump from 2969 g/cm^3 to 3350 g/cm^3. Density was estimated from velocity (Christensen and Mooney, 1995). The single strong reflection of the MTZ might suggest a sharp discontinuity at the base of the crust or arise from constructive interference between individual reflections from high and low velocity lenses of mafic and ultramafic rocks within a relatively narrow MTZ (Karson et al., 1984; Collins et al., 1986). The vertical resolution at the Moho discontinuity does not allow us to distinguish between those two models; for dominant frequencies of 7 to 15 Hz, the vertical resolution is ∼115 to 250 m.

The reflection coefficients computed for the lower crustal reflections can be used to test competing explanations for their origin, which are discussed in Section 6.1. Assuming a P-velocity of 7 km/s, dominant frequencies of 15–25 Hz indicate a vertical resolution of 35–55 m.

6. Discussion

6.1. Lower crustal dipping reflections

The most prominent and intriguing seismic structures imaged in this study are the dipping lower crustal reflections. Dipping events confined to the lower crust have been previously imaged at other locations in the Pacific (e.g., Reston et al., 1999), as well as in the Atlantic (e.g., McCarthy et al., 1988). Below we discuss accretionary and crustal aging processes invoked to explain the imaged dipping reflection events.

6.1.1. Compositional banding

Bright dipping lower crustal reflections similar to those in our images have previously been attributed to varying lithological banding caused by ridge centered crustal accretion (e.g., Ranero et al., 1997) consistent with the “gabbro glacier” model, which predicts a downward and outward ductile flow of crystal cumulates from a shallow magma lens due to gravitational forces. In this model, gabbros are deformed and rotated such that lithologic layering dips toward the spreading center with larger amount of shear strain near the base of the crust (Henstock et al., 1993; Phipps Morgan and Chen, 1993; Quick and Denlinger, 1993). The geometry of the observed dipping reflectors, some of which steepen upward before disappearing, is thus consistent with the predictions of the gabbro-glacier model. Abrupt to gradational modal layering with thicknesses from millimeters to 10's of m is a pervasive and continuous feature in the lower crustal gabbroic section of the Oman ophiolite (Pallister and Hopson, 1981; Browning, 1984; Nicolas, 1989), which was formed at fast spreading rates, and is observed in the fast spreading Pacific Crust from the Hess Deep drilling sites (Gillis et al., 2014). Laterally extensive interlayering of gabbro and wehrlite with thicknesses from 10's of m to >1 km is also reported throughout the entire Oman lower layered gabbroic section and at the base of the crust in Oman and Bay of Islands ophiolites (e.g., Pallister and Hopson, 1981; Smewing, 1981; Karson et al., 1984).

To assess the ability of compositional variations between gabbroic layers to generate reflections, we computed theoretical velocities (Hacker and Abers, 2004) from modal mineralogies for gabbro lenses at the MTZ in the Oman ophiolite (Jousselin et al., 2012) that have the same type of modal layering as the lower crustal gabbros (Kelemen et al., 1997) using a temperature of 200 °C and pressure of 0.2 GPa (expected values at the base of 50-my-old oceanic crust, McKenzie et al., 2005). The maximum reflection coefficient calculated for the contrast between any of these compositions is ∼0.062 ($Vp_1 = 7.42$ km/s, $\rho_1 = 2.93$ g/cm^3 and $Vp_2 = 6.91$ km/s, $\rho_2 = 2.78$ g/cm^3, where Vp is P-wave velocity and ρ is density). In this case, velocity and density contrasts within the modally layered olivine gabbro are not sufficiently large to explain the reflection coefficient of 0.15 estimated for the brightest event. However, it is possible that thin-bed tuning effects created by closely spaced reflecting interfaces, for which reflections would interfere constructively, could significantly enhance the reflection strength. The maximum constructive interference (quarter

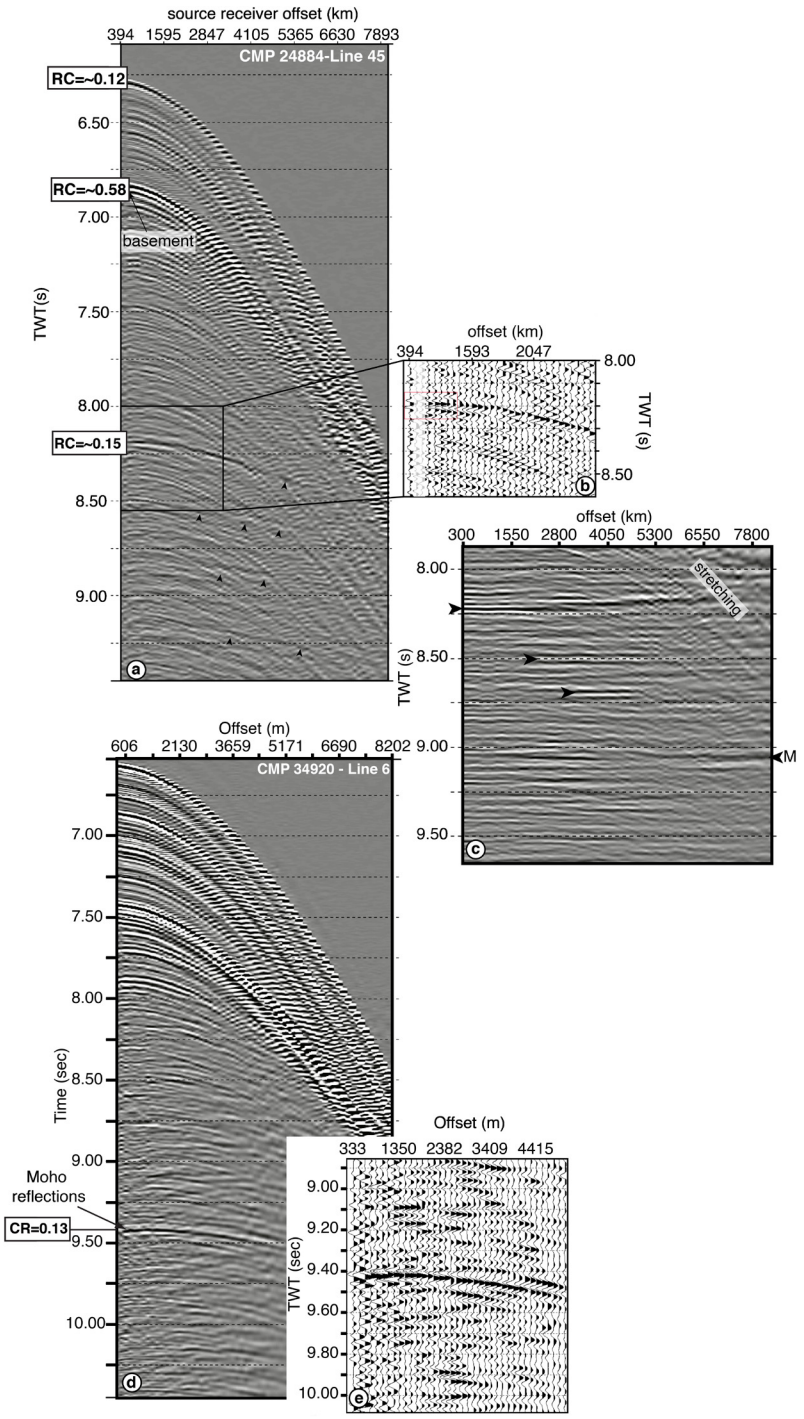

Fig. 6. (a) CMP gather #24 884 from Line 45 across fast spread crust, which comprises 64 traces, with a maximum source receiver offset of 8 km. A bright lower crustal dipping event present at ~8.20 s twtt on the near offset traces is used for reflection coefficient estimation. White boxes show the reflection coefficients (RC) after applying a correction term for attenuation. (b) Details of the dipping events on the near traces are shown using wiggle and variable area plot. (c) Part of the CMP gather displayed after pre-stack migration. Black arrows indicate the dipping event reflections and the arrow annotated with an M indicates the MTZ. (d) CMP gather #34 920 from profile 6 showing strong reflection from the MTZ at ~9.4 s twtt. White boxes on the left indicate the reflection coefficient that has been measured for the MTZ taking into account the attenuation effect. (e) Details of the MTZ reflection observed at near offset shown using a wiggle and variable area plot.

of the wavelength) would occur for thicknesses of 70 to 115 m for dominant frequencies of 15–25 Hz assuming a velocity of 7 km/s, which is thicker than observed modal layering in ophiolites and drill sites.

Mafic/ultramafic banding in the lower crust would be associated with larger contrasts in acoustic properties than predicted for modal layering in olivine gabbro, and synthetic modeling demonstrates that it can produce strong reflections (e.g., between layered gabbro ($Vp = 6.7$–7.3 km/s), wehrlite ($Vp = 7.9$–8.4 km/s), dunite ($Vp = 8.2$–8.7 km/s), harzburgite ($Vp = 8.1$–8.5 km/s), Collins et al., 1986). The contrast between the gabbro and wehrlite would produce a reflection coefficient of 0.115 (Collins et al., 1986). This could explain the lower crustal reflections and/or the MTZ where it is wide and complex (Fig. 2b, CMP 28 800–29 800). However, to explain the bright, continuous and sharp reflection that marks the MTZ over most fast-spreading lithosphere imaged by our sur-

vey, the layering would need to be confined to a narrow depth range.

6.1.2. Shear zones formed near the mid-ocean ridge

Lower crustal dipping reflections have also been interpreted as secondary shear zones induced in the ductile lower crust by near ridge-axis active mantle flow (e.g., Ranero et al., 1997; Reston et al., 1999; Kodaira et al., 2014). In this model, differential motion between the upper mantle and lower crust causes a broad area of deformation in the lower crust. This model predicts shear structures to dip towards the ridge axis and a lack of offset at the Moho. Kodaira et al. (2014) report large anisotropy in the P-wave mantle velocity with the faster axis in the downdip direction of the reflection events, which they interpret to arise from active and rapid mantle upwelling that could create secondary shear zones within the ductile lower gabbros. However, theory and modeling predict that passive flow is the dominant process for oceanic lithosphere formed at fast-spreading rates (Parmentier and Phipps Morgan, 1990; Blackman and Kendall, 2002).

If lower crustal reflections represent shear zones, their shallowest extent and length should be controlled by the depth to the brittle–ductile transition and the size and shape of the mush zone (e.g., Reston et al., 1999). The brittle–ductile transition at fast-spreading ridges roughly corresponds to the 750° isotherm and is located 1–2 km below the seafloor at the ridge axis (~380–760-ms twtt assuming 5.2 km/s) (Chen and Morgan, 1990; Phipps Morgan and Chen, 1993), and it increases to 2–3 km (~1–1.2 s twtt) below the seafloor a few kilometers off-axis due to cooling. The predicted off-axis depth best matches the depth of lower crustal events in our data. Shearing within the lower crust might occur progressively over large distances, starting in the mush zone, and continuing to develop until the gabbro reaches the brittle/plastic transition at ~750–800° (Hirth et al., 1998). Some studies suggest that there would no longer be melt (and thus shearing would stop) at as close as 5 km from the ridge axis (e.g., Cherkaoui et al., 2003), but other models maintain high temperatures in the lower crust to distances much greater than 5 km from the ridge (e.g., Henstock et al., 1993). The spatial concentration of interstitial melt fraction diminishes with distance from the axis. When the fraction of melt is too high near the ridge axis, or when the zone with interstitial melt is too narrow at the edges of the mush zone, shear zones cannot develop. The shape and size of the zone with interstitial melt (thermal boundary layer >1150 °C) and amount of melt present could control the formation and evolution of shear zones and may partially explain why lower crustal reflections have not been imaged right beneath the ridge axis.

Another process that may contribute to the formation and preservation of lower crustal shear zones is stress-driven melt segregation. Melt segregation at high temperatures and pressures has been observed in experiments at small scales but can be extrapolated to larger scales (Holtzman et al., 2003; Holtzman and Kohlstedt, 2007). Such melt segregation could result in compositional differences between the shear zones and the surrounding lower crust.

Ophiolite studies have also shown that active mantle upwelling, with the mantle moving away from the ridge faster than the crust, may impose a basal shear on the crust (Nicolas et al., 1994). However, shear zones with scales similar to the lower crustal reflections that we image have not been observed to date in ophiolites.

6.1.3. Post accretion processes

Lower crustal dipping reflections similar to those presented here have never been imaged near the ridge axis or in very young oceanic crust (<5 Myr), which has led to alternative explanations for their formation rooted in off-axis processes, such as late faulting and fracturing, or off-axis magmatism (e.g., Hallenborg et al., 2003).

In the hypothesis that dipping events represent late faults, their reflectivity would be acquired by damage (brecciation) and/or fluid migration and rock alteration along the faults. Alteration products within fault zones can produce significant changes in the impedance contrast (e.g., Jones and Nur, 1984). Late faulting could be caused by, for example, thermoelastic stresses (e.g., Parmentier and Haxby, 1986). However, the following observations counter the interpretation of dipping lower crustal structures as late faults: scarps at the top of the basement do not match upward-projected lower crustal reflections; these events have lower dips than expected for normal faults; offset are not observed at the MTZ. Finally, the observation that lower crustal events sole into the MTZ implies that they likely developed at the same time as the MTZ (e.g., Ranero et al., 1997; Reston et al., 1999), and thus at or near the ridge axis (Detrick et al., 1993).

Alternatively, dipping reflectors formed at or near the ridge axis due to shearing or compositional banding could be later "illuminated" by off-axis hydrothermal circulation along fault zones. However, our data show only minor faulting imaged within the sediment cover that could provide pathways for seawater to the upper crust, and our data do not image structures that penetrate from the basement to the lower crust that could be sufficient pathways for deeper hydration and off-axis illumination.

Off-axis magmatism is also unlikely to be the cause for the dipping reflectivity. Substantial off-axis volcanism tends to add volcanic constructions (e.g., seamounts) in the upper crust, but the lower crustal dipping events are better imaged when the basement is smooth. Additionally, the crustal thickness is relatively constant along all the profiles with dipping events, suggesting that off-axis magmatism, which would potentially increase crustal thickness, has been minimal or uniform but has not had an impact on the reflectivity of the lower crust.

6.1.4. Summary of preferred interpretation

We favor the interpretation of dipping events as frozen macroscopic ductile deformation of a zone of crystal cumulates that contains interstitial melt due to active mantle upwelling, consistent with previous studies (e.g., Kodaira et al., 2014). However, as described below, we propose new mechanisms for the reflectivity of the events and a new view of their implications for conditions at the mid-ocean ridges that created them (Section 6.3).

The bright reflections (RC ~ 0.15) originating from these shear zones are difficult to explain assuming simple specular reflections. Strong lower crustal dipping reflectivity could be enhanced by anisotropy caused by alignment of fabric within the shear zones (Reston et al., 1999). Another possible contribution to the reflectivity briefly mentioned in previous work, is melt concentration within shear zones (Reston et al., 1999; Hallenborg et al., 2003), which can also lead to compositional variations.

Melt trapped within the shear zones will probably crystallize to form oxide gabbros from late Fe–Ti rich melt such as ferrogabbros (e.g., Natland and Dick, 1996), which have a higher density (~3.2 g/cm^3) but lower velocity (Vp = ~6.75 km/s) than undeformed olivine gabbros (Vp = ~7.3 km/s, ρ = 3 g/cm^3) (Birch, 1961; Iturrino and Christensen, 1991; Iturrino et al., 1991). The velocity and density difference between the oxide-rich gabbro filling the shear zones and the adjacent gabbros could thus contribute to, but not be solely responsible for, the large reflection coefficient (R.C. ~ 0.15) estimated from reflections arising at these shear zones.

Another process that can lead to increased reflectivity of shear zones is mylonitization, which changes the grain size and reduces the velocity (Iturrino and Christensen, 1991). Compositional heterogeneity arising from mylonitization could also con-

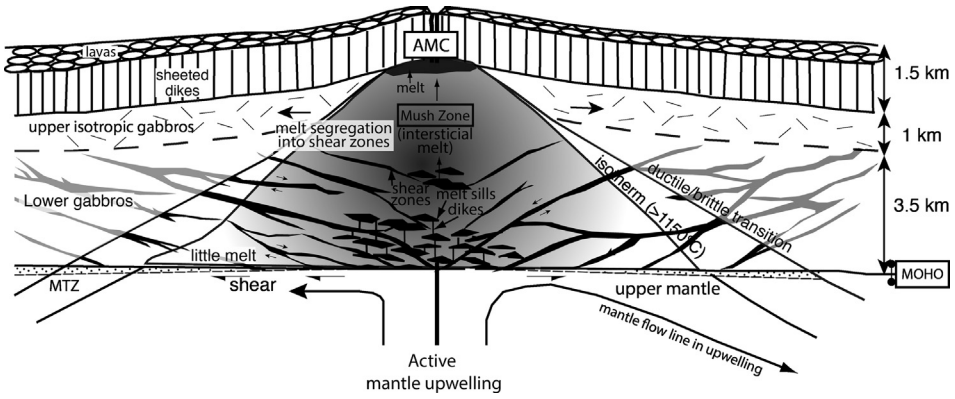

Fig. 7. Cartoon showing the proposed model for the generation of lower crustal dipping events. Dipping reflectors are secondary shear zones formed in the ductile lower crustal zone with interstitial melt segregated into these shear zones. The isotherms 1150 and 700° are shown schematically. The bright reflectivity (RC = ~0.15) of these shear zones can be explained by a combination of compositional differences of the melt segregation into these shear zones, crystal anisotropy, change of mineral content through mylonization, and constructive interference.

tribute to variations in the strength of the imaged reflections. Mylonitization could also lead to preferred crystalline orientation of anisotropic minerals producing a strong reflection coefficient (Christensen and Szymanski, 1988; Iturrino et al., 1991), but anisotropy is also unlikely to account for the high reflection coefficient alone (Christensen, 1978). The remarkably strong reflections observed in our study thus likely originate from a combination of variations in composition, mineral alignment and constructive interference in mylonites.

Cross-cutting relationships are observed in some areas. These could represent dipping events cut by later faults or an anastomosing network with larger bands at higher angles connected by smaller bands at lower angles (Holtzman and Kohlstedt, 2007), which our data cannot resolve (Fig. 7). This could explain observed differences in the distribution of the dipping events, from discrete features with a regular spacing (e.g., Ranero et al., 1997), to a more complicated network (Hallenborg et al., 2003). Morphology and organization of the anastomosing network (thickness, angle, spacing, volume fraction, and melt fraction) depends on the driving force, permeability and melt viscosity. It is also possible that some complex geometries could be caused by out-of-plane surface scattering events, but this cannot explain all of our observations.

6.2. Moho transition zone and uppermost mantle reflections

We also observe events in the uppermost mantle that primarily dip gently away from the ridge axis, which is in the opposite direction of lower crustal reflections. Sub-crustal events that dip toward the ridge axis have been observed elsewhere and interpreted as frozen gabbro lenses and melt accumulations embedded within mantle rocks (Nedimović et al., 2005). Mafic intrusions embedded in harzburgite or dunite have been observed in the Oman ophiolite (Benn et al., 1988; Boudier and Nicolas, 1995; Jousselin and Nicolas, 2000). Gabbro megalenses might be large-scale features (>3 km long and up to 100 m thick) (Karson et al., 1984; Benn et al., 1988) and may have locally steep dips relative to the Moho because of the intense deformation of the mantle by solid-state flow away from the ridge axis.

The OBS wide-angle refraction traveltime modeling in our area shows no reduction in the uppermost mantle velocity or apparent increase of the crustal thickness that would be associated with mafic intrusions embedded in mantle rocks or with serpentinization (Shillington et al., 2013). The absence of old or active faults cutting the entire crust also argue against serpentinization.

We thus propose that these events might also represent shear zones within the uppermost mantle formed near the ridge axis, where shearing is localized at the MTZ. Like the lower crustal dipping structures, mantle shear zones may be reflective due to a combination of compositional variations caused in part by melt segregation within the shear zones (e.g., olivine + chromite) (Holtzman et al., 2003) and/or mineral alignment resulting from deformation.

6.3. Models for formation of dipping lower crustal structures

6.3.1. Spreading rate

Dipping events restricted to the lower crust have been described in fast to ultra-fast spreading oceanic crust in the Pacific Ocean (Eittreim et al., 1994; Ranero et al., 1997; Reston et al., 1999; Hallenborg et al., 2003; Kodaira et al., 2014). However, in some places along the 6100-km-long Pacific transect of Eittreim et al. (1994), lower crustal dipping events have been also imaged in crust formed at a moderate spreading rate (~30 mm/yr, half rate). This transect was acquired with a shorter streamer and was processed in a simpler way than profiles published afterwards, i.e. without pre or post-stack time migration. Eittreim et al. (1994) image dipping events every 50–100 km, including near the East Pacific Rise where modern 2D and 3D MCS experiments have not imaged any such events (e.g., Han et al., 2014). A recent study by Han et al. (2013) imaged lower crustal dipping events in the Juan de Fuca oceanic crust that are similar to the events observed in the oceanic crusts in Alaska and in the NE Pacific (e.g., Ranero et al., 1997). The Juan de Fuca oceanic crust was also formed at an intermediate spreading rate (~38 mm/yr, half rate) (Wilson et al., 1984). Furthermore, dipping events restricted to the lower crust that share some of the same characteristics as those imaged for fast spreading crust have been reported in the Central Atlantic Ocean (McCarthy et al., 1988; White et al., 1990; Morris et al., 1993). These sections of crust were accreted at a half rate of ~20 mm/yr, which is slow but sufficient for the lower crust to be ductile (Chen and Morgan, 1990; Phipps Morgan and Chen, 1993) allowing shear zones to develop near the ridge axis. These sections also have unusually large crustal thicknesses (~7–8 km) (Morris et al., 1993), anomalously smooth basement topography (Minshull, 1999) and brighter than normal Moho reflections. These observations are similar to those reported in our study and elsewhere where reflections are observed, which could support a common origin for the dipping events and imply that spreading rate, alone, does not control where they form.

6.3.2. Normal versus anomalous spreading

Secondary shear zones in the lower crust require that the mantle is moving faster in the flow line direction than the overriding

lower ductile crust, at least locally beneath the zone with interstitial melt. However, magmatic processes associated with passive upwelling have been suggested to be the dominant process at fast spreading rates (e.g., Phipps Morgan and Forsyth, 1988; Parmentier and Phipps Morgan, 1990; Blackman and Kendall, 2002), where the predicted mantle flow is close to spreading rate. This suggests that shearing in the lower crust may be associated with an anomalous spreading activity. Kodaira et al. (2014) interpreted strong P-wave anisotropy in the uppermost mantle as evidence for active mantle upwelling in the flow line direction in a region where dipping reflections are observed and suggest that this might be a common phenomenon at fast-spreading rate. We propose an alternative possible explanation that anomalous conditions may have existed at the mid ocean ridge arising from plate reorganization or from a distant plume influence that could locally produce a more active and complex (three dimensional) viscous mantle flow (Blackman and Kendall, 2002) capable of producing lower crustal shear zones.

In this study, the dipping events have been imaged for crust formed at chron 24 (~53–55 Ma), when a major plate reorganization took place. This major plate reorganization is associated with rotation of the Kula–Pacific spreading direction and a jump in the Kula–Pacific–Farallon triple junction located ~100 km away from the MCS profiles (Lonsdale, 1988) (Fig. 1). We thus propose that this plate reorganization could have locally produced more active mantle flow. Dipping events are not imaged for crust formed at intermediate spreading rate after plate reorganization had stopped (chrons 21–23).

Likewise, other regions where dipping events are observed are associated with similar reorganizations. Dipping events in the lower crust over a bright Moho in the Juan de Fuca plate only occur in an 8-my-old segment of the crust (Han et al., 2013) accreted when a plate reorganization took place (Wilson et al., 1984). Dipping events in the Cocos lower crust (Hallenborg et al., 2003) are observed in the 15–17 Ma crust formed at the East Pacific Rise (EPR) between the Pacific and Cocos Plates in the vicinity of the Cocos–Nazca–Pacific triple junction and Galapagos hotspot (e.g., Meschede et al., 1998; Barckhausen et al., 2008). The Cocos–Nazca spreading center has a complex history including several reorganizations and ridge jumps (e.g., at 19.5 and 14.5 Ma) towards the Galapagos hotspot system (~150 km away).

At the time of accretion of the NW Pacific crust containing dipping reflectors (Ranero et al., 1997; Reston et al., 1999; Fujie et al., 2013; Kodaira et al., 2014), the Izigani–Pacific ridge was located ~500–1000 km from the Ridge–Ridge–Ridge triple junction and the Shatsky hotspot (Nakanishi et al., 1999). From Chrons M12 to M4, at least four ridge jumps occurred that were related to the presence of the hotpost near the triple junction or associated with major reorganization of the ridge (Farallon–Pacific, Pacific–Izanagi).

At the time of the crustal accretion of Western Atlantic oceanic crust with similar dipping events (e.g., McCarthy et al., 1988; Morris et al., 1993), several plate reorganizations are proposed to have occurred at 170 Ma at the Blake Spur Magnetic Anomaly, including a ridge jump and/or a major change in the direction and speed of spreading (e.g., Klitgord and Schouten, 1986; Schettino and Turco, 2009; Labails et al., 2010); other events may have also occurred at 154 Ma (Labails et al., 2010) and 132 Ma (White et al., 1990).

Dipping lower crustal events are not reported in MCS profiles acquired seaward of the outer-rise region of the Chilean subduction zone (Contreras-Reyes et al., 2007). This is an example of mature crust formed at fast-spreading rates away from any plate reorganizations where no dipping events have been imaged. Likewise, dipping lower crustal structures are not observed at studied active mid-ocean ridges, up to 85 km away from the EPR in some places (Barth and Mutter, 1996), or in ophiolites.

In summary, the regions where lower crustal events are imaged appear to be associated with unusual accretionary processes arising from plate reorganizations with ridge jumps or ridge propagation or from distant plumes. The impact of plate organizations on mantle flow is poorly known. Previous modeling and observational studies suggest that plate reorganizations, distant plumes, and ridge reorientations and migrations could be associated with variations in mantle flow patterns (Blackman and Kendall, 2002; Carbotte et al., 2004; Seton et al., 2015). Our results imply that these events could be associated with episodic, focused and local upwelling of the mantle due to changes in upwelling rate, effective viscosity, or other properties, or by changing relative velocities between the crust and mantle due to, for example, ridge migration.

However, this study cannot exclude the possibility that the dipping events result from mafic/ultramafic banding. As mentioned earlier, mafic/ultra-mafic layering is able to produce large impedance contrasts, and the observed geometries of the dipping events are in part consistent with the predictions of the "gabbro glacier" model (e.g., Henstock et al., 1993). In this case, plate reorganization could also explain the discrete character of the dipping events by generating small, periodic, and relatively mafic magmatic pulses. Magmatic pulses have been linked to a global scale plate reorganization (e.g., Matthews et al., 2012) but could exist at a smaller scale.

Thus we speculate that specific events may promote or be required for the formation of dipping events in the lower crust. More observations are needed in old oceanic crust to test possible controls, particularly for normal (7-km-thick) old oceanic crust accreted away from plate reorganizations.

7. Conclusions

We analyze new MCS reflection data across fast spread Eocene Pacific oceanic crust offshore Alaska that contains dipping reflections confined to the lower oceanic crust. We propose that these dipping events are accretionary structures that form in shear zones and have a hybrid tectonic and magmatic origin. Our preferred model can account for the characteristics and occurrence of lower crustal dipping reflections off Alaska and elsewhere. However, we cannot completely exclude the alternative possibility that they arise from magmatic layering alone.

1. The strong amplitude of lower crustal reflections (CR ~ 0.15) can be explained by a combination of stress-driven melt segregation, mylonitization and crystal alignment (anisotropy) within the shear zones in the ridge area characterized by interstitial melt. The length of the reflection events is related to the size and shape of the zone with interstitial melt and the brittle–ductile isotherm.
2. The lack of offsets at Moho, confinement of reflections to the lower crust, and small dip ($<30°$) suggests that these events are not caused by faulting. Limited faulting of sediment suggests that late illumination by fluid percolation is also unlikely.
3. The dipping lower crustal reflections are observed worldwide in crust formed at a range of spreading rates, implying that spreading rate, alone, does not control their formation.
4. The formation of lower crustal shear zones requires shear at the base of the crust. We speculate that plate reorganizations could produce local and focused active mantle upwelling within the axial zone and thus cause differential motion at the base of the crust. This could explain why the lower crustal dipping events are observed in a variety of spreading rates

and why they are not observed at modern intermediate to fast spreading ridges or in many other regions away from the ridge axis. Thus, lower crustal dipping reflections may not be a general feature of fast spreading crust.

Acknowledgements

We thank the Captain, scientific technical staff and crew of the R/V *Marcus G. Langseth* for the acquisition of the data and Ben Holtzman, Suzanne Carbotte, Shuoshuo Han for illuminating discussions. This work was supported by the National Science Foundation (NSF) grant OCE-0926614. We thank two anonymous reviewers for their helpful comments and suggestions.

Appendix A. Supplementary material

Supplementary material related to this article can be found online at http://dx.doi.org/10.1016/j.epsl.2015.05.016.

References

Barckhausen, U., Ranero, C.R., Cande, S.C., Engels, M., Weinrebe, W., 2008. Birth of an intraoceanic spreading center. Geology 36, 767–770. http://dx.doi.org/10.1130/G25056A.1.

Barth, G.A., Mutter, J.C., 1996. Variability in oceanic crustal thickness and structure: multichannel seismic reflection results from the northern East Pacific Rise. J. Geophys. Res. 101, 17951. http://dx.doi.org/10.1029/96JB00814.

Bécel, A., Shillington, D.J., Nedimović, N.R., Kuehn, H., Webb, S.C., Holtzman, B.K., 2012. Seismic structure of the North Pacific oceanic crust prior plate bending at the Alaska subduction zone. In: AGU Fall Meeting Abstracts, vol. 1. 2702, bibliographic code: 2012AGUFM.T13G2702B.

Bée, M., Bibee, L.D., 1989. A seismic refraction study of cretaceous oceanic lithosphere in the Northwest Pacific Basin. Mar. Geophys. Res. 11, 239–261. http://dx.doi.org/10.1007/BF00282578 (Figure 2).

Benn, K., Nicolas, A., Reuber, I., 1988. Mantle–crust transition zone and origin of wehrlitic magmas: evidence from the Oman ophiolite. Tectonophysics 151, 75–85. http://dx.doi.org/10.1016/0040-1951(88)90241-7.

Birch, F., 1961. The velocity of compressional waves in rocks to 10 kilobars: 2. J. Geophys. Res. 66 (7), 2199. http://dx.doi.org/10.1029/JZ066i007p02199.

Blackman, D.K., Forsyth, D.W., 1992. The effects of plate thickening on three-dimensional, passive flow of the mantle beneath mid-ocean ridges. In: Phipps Morgan, J., Blackman, D., Sinton, J. (Eds.), Mantle Flow and Melt Generation Beneath Mid-Ocean Ridges. In: Geophys. Monogr. AGU, Washington, DC.

Blackman, D.K., Kendall, J.-M., 2002. Seismic anisotropy in the upper mantle 2. Predictions for current plate boundary flow models. Geochem. Geophys. Geosyst. 3 (9), 8602. http://dx.doi.org/10.1029/2001GC000247.

Bosch, D., Jamais, M., Boudier, F., Nicolas, A., Dautria, J.M., Agrinier, P., 2004. Deep and high-temperature hydrothermal circulation in the Oman ophiolite – petrological and isotopic evidence. J. Petrol. 45 (6), 1181–1208. http://dx.doi.org/10.1093/petrology/egh010.

Boudier, F., Nicolas, A., 1995. Nature of the Moho transition zone in the Oman ophiolite. J. Petrol. 36 (3), 777–796. http://dx.doi.org/10.1093/petrology/36.3.777.

Boudier, F., Nicolas, A., Ildefonse, B., 1996. Magma chambers in the Oman ophiolite: fed from the top and the bottom. Earth Planet. Sci. Lett. 144 (96), 239–250. http://dx.doi.org/10.1016/0012-821X(96)00167-7.

Browning, P., 1984. Cryptic variation within the Cumulate Sequence of the Oman ophiolite: magma chamber depth and petrological implications. Geol. Soc. (Lond.) Spec. Publ. 13, 71–82. http://dx.doi.org/10.1144/GSL.SP.1984.013.01.07.

Canales, J.P., Carton, H., Carbotte, S.M., Mutter, J.C., Nedimović, M.R., Xu, M., Aghaei, O., Marjanović, M., Newman, K., 2012. Network of off-axis melt bodies at the East Pacific Rise. Nat. Geosci. 5 (4), 279–283.

Carbotte, S.M., Small, C., Donnelly, K., 2004. The influence of ridge migration on the magmatic segmentation of mid-ocean ridges. Nature 429 (6993), 743–746.

Chen, Y., Morgan, W.J., 1990. Rift valley/no rift valley transition at mid-ocean ridges. J. Geophys. Res. 95, 17571–17581.

Cherkaoui, A.S.M., Wilcock, W.S.D., Dunn, R.a., Toomey, D.R., 2003. A numerical model of hydrothermal cooling and crustal accretion at a fast spreading mid-ocean ridge. Geochem. Geophys. Geosyst. 4 (9). http://dx.doi.org/10.1029/2001GC000215.

Choo, J., Downton, J., Dewar, J., 2004. LIFT: a new and practical approach to noise and multiple attenuation. First Break 22, 39–44.

Christensen, N., 1978. Ophiolites, structure seismic velocities and oceanic crustal. Tectonophysics 47, 131–157.

Christensen, N.I., Mooney, W.D., 1995. Seismic velocity structure and composition of the continental crust: a global view. J. Geophys. Res. 100, 9761. http://dx.doi.org/10.1029/95JB00259.

Christensen, N.I., Szymanski, C.L., 1988. Origin of reflections from the Brevard Fault Zone. J. Geophys. Res. 93 (B2), 1087–1102.

Collins, J.A., Brocher, T.M., Karson, J.A., 1986. Two-dimensional seismic reflection modeling of the inferred fossil oceanic crust/mantle transition in the Bay of Islands ophiolite. J. Geophys. Res. 91 (B12), 12520–12538.

Contreras-Reyes, E., Grevemeyer, I., Flueh, E.R., Scherwath, M., Heesemann, M., 2007. Alteration of the subducting oceanic lithosphere at the southern central Chile trench-outer rise. Geochem. Geophys. Geosyst. 8 (May). http://dx.doi.org/10.1029/2007GC001632.

Detrick, R.S., Harding, A.J., Kent, G.M., Orcutt, J.A., Mutter, J.C., Buhl, P., 1993. Seismic structure of the southern East Pacific Rise. Science 259 (5094), 499–503.

Dunn, R.A., Toomey, D.R., Solomon, S.C., 2000. Three-dimensional seismic structure and physical properties. J. Geophys. Res. 105, 23537–23555.

Eittreim, L., Gnibidenko, H., Sliter, R., Ragozin, N., 1994. Oceanic crustal thickness and seismic character along a central Pacific transect. J. Geophys. Res. 99 (B2), 3139–3145.

Engebretson, D.C., Cox, A., Gordon, R.G., 1984. Relative motions between oceanic plates of the Pacific Basin. J. Geophys. Res. 89 (B12), 10291–10310. http://dx.doi.org/10.1029/JB089iB12p10291.

Fisher, A.T., 1998. Permeability within Basaltic Oceanic Crust. Rev. Geophys. 36 (97), 143–182.

Forsyth, D., 1992. Geophysical constraints on mantle flow and melt generation beneath mid-ocean ridges. In: Morgan, J.P., Blackman, D.K., Sinton, J.M. (Eds.), Mantle Flow and Melt Generation at Mid-Ocean Ridges. In: Geophys. Monogr., vol. 71, pp. 1–65.

Fujie, G., Kodaira, S., Yamashita, M., Sato, T., Takahashi, T., Takahashi, N., 2013. Systematic changes in the incoming plate structure at the Kuril trench. Geophys. Res. Lett. 40, 88–93. http://dx.doi.org/10.1029/2012GL054340.

Gillis, K.M., Snow, J.E., Klaus, A., Abe, N., Adrião, Á.B., Akizawa, N., et al., 2014. Primitive layered gabbros from fast-spreading lower oceanic crust. Nature 505, 204–207. http://dx.doi.org/10.1038/nature12778.

Hacker, B.R., Abers, G.A., 2004. Subduction Factory 3: an Excel worksheet and macro for calculating the densities, seismic wave speeds, and H_2O contents of minerals and rocks at pressure and temperature. Geochem. Geophys. Geosyst. 5, 1–7. http://dx.doi.org/10.1029/2003GC000614.

Hallenborg, E., Harding, A.J., Kent, G.M., Wilson, D.S., 2003. Seismic structure of 15 Ma oceanic crust formed at an ultrafast spreading East Pacific Rise: evidence for kilometer-scale fracturing from dipping reflectors. J. Geophys. Res. 108, 1–22. http://dx.doi.org/10.1029/2003JB002400.

Han, S., Carbotte, S.M., Carton, H.D., Canales, J., Nedimović, M.R., 2013. Multichannel seismic images of Cascadia Forearc structure at the Oregon Margin. In: American Geophysical Union, Fall Meeting Abstracts. 2440, bibliographic code: 2013AGUFM.S21C2440H.

Han, S., Carbotte, S.M., Carton, H., Mutter, J.C., Aghaei, O., Nedimović, M.R., Canales, J.P., 2014. Architecture of on- and off-axis magma bodies at EPR 9°37–40′N and implications for oceanic crustal accretion. Earth Planet. Sci. Lett. 390, 31–44. http://dx.doi.org/10.1016/j.epsl.2013.12.040.

Henstock, T.J., Woods, A.W., White, R.S., 1993. The accretion of oceanic crust by episodic sill intrusion. J. Geophys. Res. 98 (B3), 4143–4161. http://dx.doi.org/10.1029/92JB02661.

Hirth, G., Escartín, J., Lin, J., 1998. The rheology of the lower oceanic implications for lithospheric deformation at mid-ocean ridges. Geophys. Monogr. 106, 291–303.

Holtzman, B.K., Kohlstedt, D.I., 2007. Stress-driven melt segregation and strain partitioning in partially molten rocks: effects of stress and strain. J. Petrol. 48 (12), 2379–2406. http://dx.doi.org/10.1093/petrology/egm065.

Holtzman, B.K., Kohlstedt, D.L., Zimmerman, M.E., Heidelbach, F., Hiraga, T., Hustoft, J., 2003. Melt segregation and strain partitioning: implications for seismic anisotropy and mantle flow. Science 301, 1227–1230. http://dx.doi.org/10.1126/science.1087132.

Iturrino, G.J., Christensen, N.I., 1991. Reflectivity modeling of the Layer 3 gabbroic sequence drilled at the Atlantis II fracture zone. In: Von Herzen, R.P., Robinson, P.T., et al. (Eds.), Proc. Ocean Drill. Program Sci. Results, vol. 118, pp. 245–251. Chapter 12.

Iturrino, G.J., Christensen, N.I., Kirby, S., Salisbury, M.H., 1991. Seismic velocities and elastic properties of oceanic gabbroic rocks from Hole 735B. In: Von Herzen, R.P., Robinson, P.T., et al. (Eds.), Proc. Ocean Drill. Program Sci. Results, vol. 118, pp. 227–244. Chapter 11.

Jones, Terry D., Nur, A., 1984. The nature of seismic reflections from deep crustal fault zones. J. Geophys. Res. 89 (4), 3153–3171.

Jousselin, D., Nicolas, A., 2000. The Moho transition zone in the Oman ophiolite-relation with wehrlites in the crust and dunites in the mantle. Mar. Geophys. Res. 21, 229–241. http://dx.doi.org/10.1023/A:1026733019682.

Jousselin, D., Morales, L.F.G., Nicolle, M., Stephant, A., 2012. Gabbro layering induced by simple shear in the Oman ophiolite Moho transition zone. Earth Planet. Sci. Lett. 331–332, 55–66. http://dx.doi.org/10.1016/j.epsl.2012.02.022.

Karson, J.A., Collins, J.A., Casey, J.F., 1984. Geologic and seismic velocity structure of the crust/mantle transition in the Bay of Islands ophiolite complex. J. Geophys. Res., Solid Earth 89, 6126–6138.

Kelemen, P.B., Koga, K., Shimizu, N., 1997. Geochemistry of gabbro sills in the crust–mantle transition zone of the Oman ophiolite: implications for the origin of

the oceanic lower crust. Earth Planet. Sci. Lett. 146, 475–488. http://dx.doi.org/10.1016/S0012-821X(96)00235-X.
Kent, M., Harding, J., Orcutf, A., 1993. Distribution of magma beneath the East Pacific Rise between the Clipperton Transform and the 9°17′N Deval from forward modeling of common depth point data. J. Geophys. Res. 98 (93), 13945–13969. http://dx.doi.org/10.1029/93JB00705.
Klitgord, K.D., Schouten, H., 1986. Plate kinematics of the central Atlantic. In: Vogt, P.R., Tucholke, B.E. (Eds.), The Geology of North America, vol. M: The Western North Atlantic Region. Geological Society of America, Boulder, CO, pp. 351–378.
Kodaira, S., Fujie, G., Yamashita, M., Sato, T., Takahashi, T., 2014. Seismological evidence of mantle flow driving plate motions at a palaeo-spreading centre. Nat. Geosci. 7, 371–375. http://dx.doi.org/10.1038/NGEO2121.
Labails, C., Olivet, J.L., Aslanian, D., Roest, W.R., 2010. An alternative early opening scenario for the Central Atlantic Ocean. Earth Planet. Sci. Lett. 297 (3–4), 355–368. http://dx.doi.org/10.1016/j.epsl.2010.06.024.
Lonsdale, P., 1988. Paleogene history of the Kula plate: offshore evidence and onshore implications. Bull. Geol. Soc. Am. 100, 733–754. http://dx.doi.org/10.1130/0016-7606(1988)100<0733:PHOTKP>2.3.CO;2.
Malinverno, A., 1991. Inverse square-root dependence of mid-ocean flank roughness on spreading rate. Nature 352, 58–60.
Matthews, K.J., Seton, M., Müller, R.D., 2012. A global-scale plate reorganization event at 105–100 Ma. Earth Planet. Sci. Lett. 355, 283–298.
McBride, J.H., White, R.S., Henstock, T.J., Hobbs, R.W., 1994. Complex structure along a Mesozoic sea-floor spreading ridge: BIRPS deep seismic reflection, Cape Verde abyssal plain. Geophys. J. Int. 119, 453–478.
McCarthy, J., Mutter, J.C., Morton, J.L., Sleep, N.H., Thompson, G.A., 1988. Relic magma chamber structures preserved within the Mesozoic North Atlantic crust? Geol. Soc. Am. Bull. 100 (September), 1423–1436. http://dx.doi.org/10.1130/0016-7606(1988)100<1423:RMCSPW>2.3.CO;2.
McCulloch, M.T., Gregory, R.T., Wasserburg, G.J., Taylor, H.P., 1981. Sm–Nd, Rb–Sr and $^{18}O/^{16}O$ isotopic systematics in an oceanic crustal section: evidence from the Samail ophiolite. J. Geophys. Res. 86 (B4), 2721–2735.
McKenzie, D., Jackson, J., Priestley, K., 2005. Thermal structure of oceanic and continental lithosphere. Earth Planet. Sci. Lett. 233, 337–349. http://dx.doi.org/10.1016/j.epsl.2005.02.005.
Meschede, M., Barckhausen, U., Worm, H.U., 1998. Extinct spreading on the Cocos Ridge. Terra Nova 10, 211–216. http://dx.doi.org/10.1046/j.1365-3121.1998.00195.x.
Minshull, T.A., Singh, S.C., 1993. Shallow structure of oceanic crust in the western North Atlantic from seismic waveform inversion and modeling. J. Geophys. Res. 98 (B2), 1777–1792. http://dx.doi.org/10.1029/92JB02136.
Minshull, T.A., 1999. On the roughness of Mesozoic oceanic crust in the Western North Atlantic. Geophys. J. Int. 136, 286–290.
Mithal, R., Mutter, J.C., 1989. A low-velocity zone within the layer 3 region of 118 Myr old oceanic crust in the wester north-Atlantic. Geophys. J. 97, 275–294.
Morris, E., Detrick, R.S., Minshull, T.a., Mutter, J.C., White, R.S., Su, W., Buhl, P., 1993. Seismic structure of oceanic crust in the western North Atlantic. J. Geophys. Res. 98, 13879. http://dx.doi.org/10.1029/93JB00557.
Mutter, J.C., Karson, J.A., 1992. Structural processes at slow spreading ridges. Science 257, 627–634.
Mutter, J.C., The NAT Study Group, 1985. Multichannel seismic images of the oceanic crust's internal structure: evidence for a magma chamber beneath the Mesozoic Mid-Atlantic Ridge. Geology 13, 629–632.
Nakanishi, M., Sager, W.W., Klaus, A., 1999. Magnetic lineations within Shatsky Rise, northwest Pacific Ocean: implications for hot spot-triple junction interaction and oceanic plateau formation. J. Geophys. Res. 104, 7539. http://dx.doi.org/10.1029/1999JB900002.
Natland, J.H., Dick, H.J.B., 1996. Melt migration through high-level gabbroic cumulates of the East Pacific Rise at Hess Deep; the origin of magma lenses and the deep crustal structure of fast-spreading ridges. In: Mével, C., Gillis, K.M., Allan, J.F., Meyer, P.S. (Eds.), Proc. Ocean Drill. Program Sci. Results, vol. 147, pp. 21–58.
NAT Study Group, 1985. North Atlantic Transect: a wide aperture, two ship multichannel seismic investigation of the oceanic crust. J. Geophys. Res. 90 (10), 321–341.
Nedimović, M.R., West, G.F., 2003a. Crooked-line 2D seismic reflection imaging in crystalline terrains: part 1, data processing. Geophysics 68 (1), 274–285. http://dx.doi.org/10.1190/1.1543213.
Nedimović, M.R., West, G.F., 2003b. Crooked-line 2D seismic reflection imaging in crystalline terrains: part 2, migration. Geophysics 68 (1), 286. http://dx.doi.org/10.1190/1.1543214.
Nedimović, M.R., Carbotte, S.M., Harding, A.J., Detrick, R.S., Canales, J.P., Diebold, J.B., Kent, G.M., Tischer, M., Babcock, J.M., 2005. Frozen magma lenses below the oceanic crust. Nature 436 (August), 1149–1152. http://dx.doi.org/10.1038/nature03944.
Nedimović, M.R., Bohnenstiehl, D.R., Carbotte, S.M., Canales, J. Pablo, Dziak, R.P., 2009. Faulting and hydration of the Juan de Fuca plate system. Earth Planet. Sci. Lett. 284, 94–102. http://dx.doi.org/10.1016/j.epsl.2009.04.013.
Nedimović, M.R., Shillington, D.J., Webb, S.C., Delescluse, M., Bécel, A., Kuehn, H., Li, J., Biescas, B., Wessbecher, A., Farkas, A., Eddy, C., Hostetler, K., Louden, K.E., 2011. Pacific plate seaward of the western Alaska trench: a view of the structure of a fossil triple junction. In: AGU Fall Meeting Abstracts, vol. 1, p. 2388.
Nicolas, A., 1989. Structures of Ophiolites and Dynamics of Oceanic Lithosphere. Kluwer Academic, Norwell, MA, 367 pp.
Nicolas, A., Boudier, F., Ildefonse, B., 1994. Evidence from the Oman ophiolite for active mantle upwelling beneath a fast-spreading ridge. Nature 370, 51–53. http://dx.doi.org/10.1038/370051a0.
Pallister, J.S., Hopson, C.A., 1981. Samail Ophiolite plutonic suite: field relations, phase variation, cryptic variation and layering, and a model of a spreading ridge magma chamber. J. Geophys. Res. 86, 2593. http://dx.doi.org/10.1029/JB086iB04p02593.
Parmentier, E.M., Haxby, W.F., 1986. Thermal stresses in the oceanic lithosphere: evidence from geoid anomalies at fracture zones. J. Geophys. Res. 91 (B7), 7193–7204. http://dx.doi.org/10.1029/JB091iB07p07193.
Parmentier, E.M., Phipps Morgan, J., 1990. Spreading rate dependence of three-dimensional structure in oceanic spreading centres. Nature 348, 325–328. http://dx.doi.org/10.1038/348325a0.
Phipps Morgan, J., Chen, Y.J., 1993. The genesis of oceanic crust: magma injection, hydrothermal circulation, and crustal flow. J. Geophys. Res. 98, 6283–6297.
Phipps Morgan, J., Forsyth, D.W., 1988. Three-dimensional flow and temperature perturbations due to a transform offset: effects on oceanic crustal and upper mantle structure. J. Geophys. Res. 93, 2955–2966.
Quick, J.E., Denlinger, R.P., 1993. Ductile deformation and the origin of layered gabbro in ophiolites. J. Geophys. Res. 98, 14015–14027.
Ranero, C.R., Reston, T.J., Belykh, I., Gnibidenko, H., 1997. Reflective oceanic crust formed at a fast-spreading center in the Pacific. Geology 25, 499–502. http://dx.doi.org/10.1130/0091-7613(1997)025<0499:ROCFAA>2.3.CO;2.
Reston, T.J., Ranero, C.R., Belykh, I., 1999. The structure of Cretaceous oceanic crust of the NW Pacific: constraints on processes at fast spreading centers. J. Geophys. Res. 104, 629. http://dx.doi.org/10.1029/98JB02640.
Schettino, A., Turco, E., 2009. Breakup of Pangaea and plate kinematics of the central Atlantic and Atlas regions. Geophys. J. Int. 178, 1078–1097. http://dx.doi.org/10.1111/j.1365-246X.2009.04186.x.
Seton, M., Mueller, R.D., Zahirovic, S., Gaina, C., Torsvik, T., Shepard, G., Talsma, A., Gurnis, M., Turner, M., Chandler, M., 2012. Global continental and ocean basin reconstructions since 200 Ma. Earth-Sci. Rev. 113 (3–4), 212–270. http://dx.doi.org/10.1016/j.earscirev.2012.03.002.
Seton, M., Flament, N., Whittaker, J., Müller, R.D., Gurnis, M., Bower, D.J., 2015. Ridge subduction sparked reorganization of the Pacific plate-mantle system 60–50 million years ago. Geophys. Res. Lett. 42 (6), 1732–1740.
Shillington, D.J., Bécel, A., Nedimović, M.R., Kuehn, H., Webb, S.C., Li, J., Keranen, K.M., Abers, G.A., 2013. Local structural controls on outer-rise faulting, hydration, and seismicity in the Alaska subduction zone. In: AGU Fall Meeting. Eos Trans. AGU, abstract T54B-06.
Smewing, J.D., 1981. Mixing characteristics and compositional differences in mantle-derived melts beneath spreading axes: evidence from cyclically layered rocks in the ophiolite of North Oman. J. Geophys. Res. 86, 2645. http://dx.doi.org/10.1029/JB086iB04p02645.
Spudich, P., Orcutt, J., 1980. A new look at the seismic velocity structure of the oceanic crust. Rev. Geophys. Space Phys. 18 (3), 627–645.
Vera, E.E., Mutter, J.C., Buhl, P., Orcutt, J.A., Harding, A.J., Kappus, M.E., Detrick, R.S., Brocher, T.M., 1990. The structure of 0- to 0.2-m.y.-old oceanic crust at 9°N on the East Pacific Rise from expanded spread profiles. J. Geophys. Res. 95 (B10), 15529. http://dx.doi.org/10.1029/JB095iB10p15529.
von Herzen, R.P., 2004. Geothermal evidence for continuing hydrothermal circulation in older (N60 M.y.) ocean crust. In: Davis, E., Elderfield, H. (Eds.), Hydrogeology of the Oceanic Lithosphere. Cambridge University Press, New York, pp. 414–447.
Warner, M., 1990. Basalts, water, or shear zones in the lower continental crust? Tectonophysics 173, 163–174. http://dx.doi.org/10.1016/0040-1951(90)90214-S.
White, R.S., 1977. Seismic bright spot in the Gulf of Oman. Earth Planet. Sci. Lett. 37, 29–37.
White, R.S., Detrick, R.S., Mutter, J.C., Buhl, P., Minshull, T.A., Morris, E., 1990. New seismic images of oceanic crustal structure. Geology 18, 462–465. http://dx.doi.org/10.1130/0091-7613(1990)018<0462:NSIOOC>2.3.CO;2.
Wilson, D.S., Hey, R.N., Nishimura, C., 1984. Propagation as a mechanism of reorientation of the Juan de Fuca ridge. J. Geophys. Res., Solid Earth 89 (4), 9215–9225. http://dx.doi.org/10.1029/JB089iB11p09215.
Zha, Y., Webb, S.C., Nooner, S.L., Crawford, W.C., 2014. Spatial distribution and temporal evolution of crustal melt distribution beneath the East Pacific Rise at 9°–10°N inferred from 3-D seafloor compliance modeling. J. Geophys. Res., Solid Earth 119, 4517–4537. http://dx.doi.org/10.1002/2014JB011131.